A Comparative Study on Thrust Map Estimation for Multirotor Aerial Vehicles

Francisco J. Anguita [1], Rafael Perez-Segui [1], Carmen DR.Pita-Romero [1], Miguel Fernandez-Cortizas [1,2], Javier Melero-Deza [1], Pascual Campoy [1] *

ABSTRACT

Precise drone flight requires stable low-level control. Direct control over the drone's collective thrust is unfeasible in most cases. A Thrust Map (TM) can be calibrated as a means of accurately actuating the motors. In this work, different approximations to a TM are evaluated to develop a general methodology for offline calibration in two steps. First, an offline estimation is obtained from experimental preflight data. Second, the offline TM is refined using a Correction Factor computed from real flight data. Different TM strategies are then discussed in terms of their performance and the resources required to compute them. Extensive experimental validation of the proposed methods has been conducted, demonstrating the effectiveness of a TM calibrated from thrust stand experiments and adjusted using the proposed correction factor. A repository with code and a video explanation are attached to help replicate this work.[1] [2]

http://www.imavs.org/

1 INTRODUCTION

Quadrotors excel for their great agility and speed. These characteristics make them ideal for demanding applications, such as drone racing or ship landing in maritime harsh environments, which require precise maneuvers [1, 2]. Such agile flight requires fast and robust low-level control, particularly attitude or rate control [3], which involves angular position (attitude), angular velocity (rates) and collective thrust commands. However, closing the control loop on thrust directly requires force sensors, increasing equipment costs and reducing flight time [4].

To avoid the drawbacks of onboard thrust sensing, quadrotors typically rely on electric propulsion systems—specifically, Brushless Direct Current (BLDC) motors—controlled through Electronic Speed Controllers (ESCs) [5]. Fuel-based propulsion systems are largely unsuitable for small quadrotors due to their weight and decreasing environmental acceptance. Flight controllers convert attitude and rate commands into throttle signals, which are normalized control inputs sent to the ESCs to actuate the rotors. Table 1 lists commonly used Flight Controller Units (FCUs) and the structure of their throttle commands.

FCU	Signal Technique	Throttle Range
Betaflight	PWM	1000-2000μs
	Oneshot	125-250μs
Ardupilot	PWM	1000-2000μs
	Oneshot	125-250μs
Pixhawk/PX4	PWM	1000-2000μs
	Oneshot	125-250μs
Crazyflie	Custom scale	10001-60000
Parrot	App slider	UI-based normalized %
Skydio	App slider	UI-based normalized %

Table 1: Throttle command encoding methods and ranges for popular flight controllers units. The *Signal Technique* indicates how throttle commands are transmitted to the ESCs, while the *Throttle Range* specifies the corresponding signal values or scales used to represent throttle percentages.

A critical component of this control chain is the relationship between the throttle input and the actual thrust produced by the rotors. The force F produced by the rotor depends on its characteristics and the angular velocity of the motor ω. This relationship can be modeled as shown in Equation 1 [6], using a thrust coefficient k_f.

$$F = k_f \cdot \omega^2 \tag{1}$$

Directly measuring this force, or estimating it from the rotor's angular speed using Equation 1, would require additional sensors mounted on the drone, which could compromise its agility.

Due to this, on most multirotors, the motors are controlled by a "throttle" command, which adjusts the duty cycle of a pulse-width modulation (PWM) signal applied to them. The actual rotational speed achieved by the motor depends not only on the throttle command but also on the battery voltage. [7].

Therefore, the formulation of the problem consists of finding a mapping function, called Thrust Map (TM), that relates the desired thrust command $T(N)$ to the throttle signal $Th(\%)$ required to achieve it, as shown in Equation 2.

*[1] Computer Vision and Aerial Robotics Group (CVAR), Centre for Automation and Robotics (C.A.R.), Universidad Politécnica de Madrid (UPM-CSIC), 28006 Madrid, Spain. Correspondence e-mail: fj.anguita@upm.es
[2] Automation and Robotics Research Group (ARG), Interdisciplinary Centre for Security, Reliability and Trust (SnT), University of Luxembourg, 1855 Luxembourg.

[1]Code repository: `https://github.com/aerostack2/thrust_map_estimation`

[2]Video: `https://vimeo.com/1104217611/ce4e5d3f6c`

$$Th = f(T, \ldots) \tag{2}$$

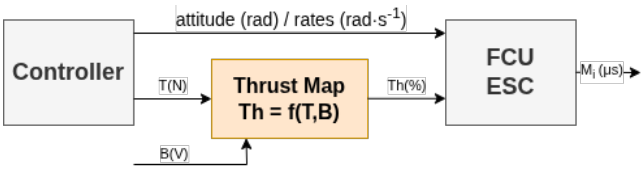

Figure 1: Block diagram of a typical thrust mapping system for quadrotor control. The low-level controller computes desired thrust values $T(N)$. These are converted into throttle commands Th$(\%)$ via a thrust map, which may depend on additional factors such as battery voltage $B(V)$. The throttle commands are then sent to the Flight Control Unit (FCU), which generates motor-specific PWM signals for actuation. These signals are transmitted to the Electronic Speed Controllers (ESCs), which regulate the power supplied to each motor, effectively controlling their speed.

Despite the importance of TM calibration, the field lacks a standardized approach to obtain and processing the data needed to build accurate maps. In this work, we focus on offline TM estimation to elaborate a detailed description of the TM calibration methods studied and report on their strengths and weaknesses based on experimental validation results. In summary, the main contributions of this work are:

1. A **comparative study** of multiple TM estimation strategies, including experimental measurements and in-flight refinements, highlighting trade-offs in accuracy and complexity.
2. A concise **methodology for offline TM estimation**, encompassing data collection, calibration, and evaluation steps.
3. A **correction procedure** that improves the accuracy of offline calibrated TMs by compensating for discrepancies observed during real flight operation.

2 RELATED WORK

TM characterization problem can be solved following two different approaches: offline calibration and online estimation. On the one hand, offline calibration refers to the process of characterizing the TM before the flight, using controlled and typically repeatable laboratory conditions. This is done by collecting thrust data through static tests (e.g., using a load cell or thrust stand) and then fitting a mathematical model—often a polynomial or surface function. On the other hand, online estimation involves determining or refining the TM during flight by using sensor data (e.g., IMU, state estimators) and real-time models. These methods dynamically adjust thrust estimates to better reflect current flight conditions, possibly adapting to changes in vehicle mass, battery level, or rotor wear.

The most extended method is the offline estimation because of its simplicity. In [8], a second-order polynomial curve is fitted to the data recorded from a motor mounted on a load cell. The work in [9] extends the 2D modeling of the TM by adding a linear dependency with the battery, thus creating a surface for the map. There are several techniques for obtaining the thrust data needed for this approach. These can be classified into direct experimental techniques, theoretical techniques, and simulation techniques.

The works in [6, 10] use commercial devices to take experimental measures of the thrust produced by the propeller. Other authors prefer to design custom thrust stands for this data recording [11]. There is, however, a general lack of description on how to process the obtained data. The work in [12] goes one step further by installing two motors onto their device in order to measure the effect of their simultaneous functioning on each other.

Regarding theoretical techniques, Classical Blade Element Theory (BET) and Blade Element Momentum Theory (BEMT) are used in [13] to obtain the force data for the map estimation. This theoretical approach is more difficult to apply to small UAVs due to aeroelastic effects and transverse flow, as described in [14].

Propeller simulation using Computational Fluid Dynamics (CFD) is an alternative to this kind of machinery. In [15, 16], CFD software is used to simulate the produced thrust data needed for the TM curves. The experimental data taken using a thrust stand is also compared to simulated CFD thrust data in [10]. However, this approach requires an accurate 3D model of the propeller, which is often not available.

No matter what method is used to gather the force or thrust measurements, it is important to note that most of the thrusts obtained using these methods are estimations, and even the experimental results may vary when all the rotors are mounted on the multirotor UAV. Regarding this matter, [8] proposes the use of a correction factor to address the difference between the estimated total thrust the multirotor will produce and the real thrust it is producing.

The problem of TM modeling can be tackled with online estimation and correction of the thrust commanded to the rotors. In [17], a BEMT-based estimator provides thrust observations for a feedforward thrust control scheme. Other techniques for online estimation of the quadrotor mass, like Least-Squares Estimation (LSE) or Extended Kalman Filter (EKF), are discussed in [18]. The thrust estimation among other parameters using a Bayesian filter is discussed in [19]. These approaches require a module to be running during flight time.

Despite the widespread use of offline TM calibration, we observe that existing work often lacks a comprehensive and reproducible methodology. In particular, there is limited guidance on how to design and conduct the necessary experiments or how to process the resulting data to obtain accurate and reliable TMs. This work addresses this gap by presenting a detailed calibration procedure that systematically covers

http://www.imavs.org/

http://www.imavs.org/

data acquisition, modeling, and evaluation, using various experimental sources.

In addition, most experimental setups used in the literature do not reproduce real flight conditions accurately. This mismatch can lead to TMs that do not generalize well to actual UAV operation. To address this, we introduce a custom extension to a commercial thrust stand to carry out experiments that better reproduce real flight conditions.

Lastly, even with careful offline calibration, discrepancies often remain between the predicted and actual thrust during flight. To mitigate this issue, we propose the addition of a correction factor in our procedure, similar to existing solutions in the literature, that refines the thrust estimation.

3 THRUST MAP CALIBRATION

3.1 Problem formulation

As mentioned in Section 1, the problem of TM calibration is the problem of approximating a function of the form described in Equation 2. This approximation can be carried out using different methods, including:

- Linear approximation.
- Polynomial approximation.
- Polynomial approximation with a correction factor.

The error committed by each method can be evaluated as the difference between the real throttle command sent during real operation, Th, and the throttle value predicted by the TM function, $\hat{Th}$, as shown in Equation 3:

$$e_{Th} = \left| Th - \hat{Th} \right| \tag{3}$$

3.2 Lineal approximation

Assuming a simplified model, the throttle signal Th can be considered a function of the desired thrust T as:

$$Th = f(T) \tag{4}$$

Under the assumption of a linear relationship between throttle and thrust, the TM function $\hat{f}$ can be approximated by a first-order expression:

$$f(T) = a \cdot T + b \tag{5}$$

where a and b are constants that define the slope and offset of the mapping. This model implies that when $T = 0$, the throttle is at its minimum value, and when $T = T_{\text{max}}$, the throttle reaches 100%.

In the particular case where the thrust-to-throttle ratio is constant and no offset is needed, the model can be further simplified as:

$$f(T) = \frac{1}{T_{\text{max}}} \cdot T \tag{6}$$

This simplification assumes that T_{max} is the maximum thrust generated when the throttle is fully applied (100%).

3.3 Polynomial approximation

To improve accuracy, the linear model can be extended by considering the influence of battery voltage on the available motor power. As the battery voltage drops, the motors' ability to generate thrust for a given throttle input decreases [20]. Therefore, a more realistic model considers both the desired thrust T and the current battery level B (in volts) as inputs.

$$Th = f(T, B) \tag{7}$$

In this work, the function f is approximated using data collected from experimental measurements, consisting of triplets of the form $Ds_i(T_i, B_i, Th_i)$ for $i = 1, \ldots, N$. These measurements represent the throttle value required to achieve a specific thrust at a given battery level. The procedure for collecting this dataset is described in Section 4.

To approximate f, a polynomial surface fitting approach is adopted. This model allows the throttle to vary smoothly with both thrust and battery level. The fitted function $\hat{f}$ is chosen from the space of bivariate polynomials of degree d, and is constructed by minimizing the total approximation error over all N data points in P.

$$\hat{f} = \underset{f \in \mathcal{P}_d}{\operatorname{argmin}} \sum_{i=1}^{N} |Th_i - f(T_i, B_i)| \tag{8}$$

Mathematically, the problem consists of finding the TM polynomial function $\hat{f}$ that minimizes the total fitting error.

3.4 Correction factor

The throttle value computed by the fitted TM function $\hat{f}(T, B)$ is responsible for generating the desired force through the drone's propulsion system. Ideally, if $\hat{f}$ were perfectly calibrated, the force produced by the drone would exactly match the thrust commanded by the controller.

However, as discussed in [8], discrepancies may arise between the expected thrust, predicted by the fitted model, and the actual thrust generated by the motors during flight. These discrepancies can arise due to in-flight effects.

To compensate for this issue, we introduce a correction factor γ. This dimensionless factor adjusts the thrust command before it is passed to the TM $\hat{f}$. The goal is to ensure that the final throttle output yields a force that matches more closely the intended thrust of the controller. This modified structure is depicted in Figure 2.

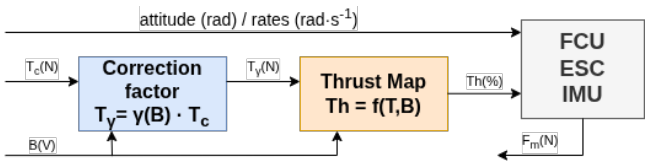

Figure 2: Diagram of the approach including the TM and the correction factor γ and the IMU that takes the acceleration measures to compute F_m, derived from Figure 1.

http://www.imavs.org/

The corrected model is formulated as:

$$Th = \hat{f}(T_\gamma, B) = \hat{f}(\gamma(B) \cdot T_c, B) \tag{9}$$

For its computation, a dataset is collected using experimental measurements, consisting of triplets $Df_j(B_j, T_{c_j}, F_{m_j})$, for $j = 1, \ldots, N$, where T_{c_j} is the thrust command passed to the TM, and F_{m_j} is the measured z-force obtained, using the vertical acceleration of the drone a_z and mass m.

For each data point, the correction factor is estimated as:

$$\gamma_j = \frac{T_{c_j}}{F_{m_j}} \tag{10}$$

Then, a univariate polynomial of degree d is fitted to the data for solving the following minimization problem:

$$\hat{\gamma}(B) = \underset{\gamma \in \mathcal{P}_d}{\operatorname{argmin}} \sum_{j=1}^{N} \left| \frac{T_{c_j}}{F_{m_j}} - \gamma(B_j) \right| \tag{11}$$

This correction function $\hat{\gamma}(B)$ enables the system to dynamically adjust the input to the TM according to the battery level, ensuring that the resulting throttle command continues to produce a thrust consistent with the original intent of the controller.

4 EXPERIMENTAL VALIDATION

To obtain the triplets of data Ds and Df described in Section 3, experiments of two different natures are designed.

Firstly, thrust stand experiments are conducted to obtain the values for throttle commanded, thrust measured and battery level of triplet Ds, to estimate a TM using the Linear Approximation (LA) and the Polynomial Approximation. Using the Polynomial Approximation, two TM strategies will be followed: experiments with one rotor only will result in a Single Rotor (SR) TM, and experiments using all of the four rotors will be used to calibrate a Multirotor (MR) TM.

Then, using the SR and MR TMs, real flight experiments are carried out to obtain the Df triplets, with thrust commanded, battery level and z force measured, which allow us to compute a correction factor for these two TMs, obtaining the Single Rotor with correction factor (SR+γ) and Multirotor with correction factor (MR+γ).

Table 2 summarizes the types of experiments and the different TM approximations and strategies.

4.1 Experimental Setup

The TMs in this work are all calibrated for an xNova BlackThunder 2207-2100Kv racing motor connected to a Foxeer Reaper F4 65A ESC and powered by a TATTU R-LINE 6S LiPo battery. To obtain the data, these components are mounted on a commercial TYTO Robotics Series 1585 thrust stand. This device has three force gauges and an electronic board that measures the force and torque produced by the motor installed on it and stores the data, thus obtaining the Ds triplet to calibrate the SR TM. To perform four rotor experiments that better replicate real drone flight conditions, an extension is mounted and connected to the thrust stand signal output. This configuration allows to compute the MR TM with the new Ds triplet obtained. Figure 3 shows the full setup for the thrust stand experiments.

Experiment Type	TM Approximation	TM Strategy
Thrust Stand	Linear	LA
	Polynomial	SR MR
Flight Experiments	Polynomial + γ	SR+γ MR+γ

Table 2: Summary of data source experiments and their related TM strategies. The thrust stand experiments allow to compute a Linear, SR and MR approximated TMs. Flight Experiments allow to apply a correction factor γ to SR and MR TMs.

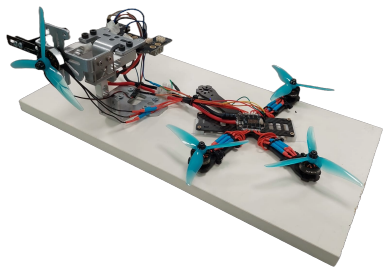

Figure 3: Commercial TYTO Robotics Series 1585 thrust stand and custom extension for multirotor experiments.

For real flight experiments, the same motors, ESC, and batteries were mounted on a 250 mm carbon fiber quadrotor frame. The ESC is controlled by a Foxeer H7 MPU6000 Flight Controller Unit (FCU). An Nvidia NX Orin is the onboard computer responsible for autonomous flying, and an Intel RealSense T265 camera is used for localization. The drone is shown in Figure 4.

Figure 4: Autonomous drone used for real flight experiments.

In terms of autonomy, the computer onboard runs Aerostack2 [21]. This open-source framework performs the state estimation, computes the control, and sends the com-

http://www.imavs.org/

mands to the FCU to carry out specified tasks using its own mission planner. The controller used is a Model-Based Predictive Controller (MPC).

4.2 *Thrust stand experiments for TM calibration*

Series of three different types of experiments were carried out on the thrust stand in the form of steps and ramps (see Figure 5) that test both the transient and steady-state behavior of a single rotor.

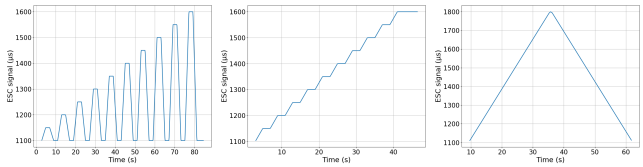

Figure 5: Sets of experiments conducted on the thrust stand to cover different operational points.

These same experiments were repeated with the four rotors connected to the ESC and commanded to rotate at the same speed and at the same time, recording a new set of data to which the new MR TM can be approximated.

With a simple experiment sending a maximum throttle command to the rotor, the maximum thrust that the rotor can produce is obtained, and thus the LA TM can be approximated using Equation 5.

Different polynomial surface alternatives are fitted to the data and tested using the error described in Equation 3 to find the surface that fits the best. Table 3 shows the error computed for each polynomial surface fit.

Polynomial	Error for SR	Error for MR
2nd degree	1.541 $\pm$ 1.936	1.009 $\pm$ 1.691
2nd deg. truncated	1.543 $\pm$ 1.956	1.041 $\pm$ 1.651
3rd degree	**1.411** $\pm$ **1.813**	**0.933** $\pm$ **1.390**
3rd deg. truncated	1.494 $\pm$ 1.886	1.009 $\pm$ 1.691

Table 3: Mean fitting error (%) computed for different degree polynomial surfaces fitted to the experimental data for SR and MR

Despite having a slightly lower error, the third degree polynomials overfit to the data for the throttle range that is being considered in this fitting process. A second degree polynomial is chosen as the best fit for the data in both cases, resulting in a TM function of the form:

$$Th = f(T, B) = a + b \cdot T + c \cdot B + d \cdot T^2 + e \cdot T \cdot B + f \cdot B^2 \quad (12)$$

The fitted surfaces that characterize the SR TM and the MR TM are shown in Figure 6.

4.3 *Flight experiments for correction factor computing*

This factor was estimated off-board using data collected in D_f from two different flight experiments for each TM to be corrected (SR and MR). For each TM, two flights are performed: one long hover flight for the entire duration of the battery, and a flight with several short hover maneuvers at different heights. This way, distinct forces are required from the rotors, increasing the variety of the data. The same flight experiments are then performed to test the SR+γ and MR+γ TMs, as well as the performance of the SR and MR TM.

The measured force, $F_m = f(a_z, m)$, was computed using the z-axis acceleration measured by the IMU and the drone's mass. As expected, the experiments showed that even though the measured thrust must be constant while the drone hovers, the requested thrust increases as the battery level decreases.

Different datasheet of correction factors were computed for the various TMs. These factors were then fitted to the most suitable curve. The goal was to minimize the error (Equation 3) to find the best degree and form of the polynomial curve.

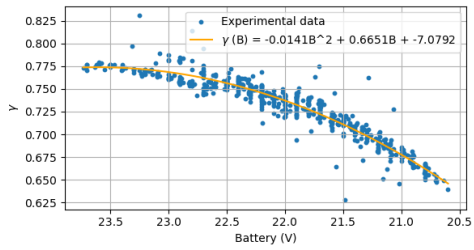

(a)

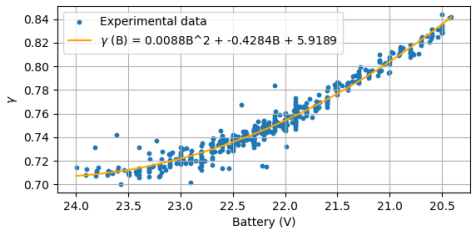

(b)

Figure 7: correction factor γ curves fitted to the data obtained from flight experiments. 7a shows the curve fitted to apply γ to the SR TM. 7b shows the curve fitted to apply γ to the MR TM.

Initially, a linear approximation dependency was used. However, this was not the best fit, so second- and third-degree approximations were tried. The results were very similar for both cases, so the second-degree polynomial approximation 13 was used to simplify the algorithm.

$$\gamma(B) = \gamma_0 + \gamma_1 \cdot B + \gamma_2 \cdot B^2 \quad (13)$$

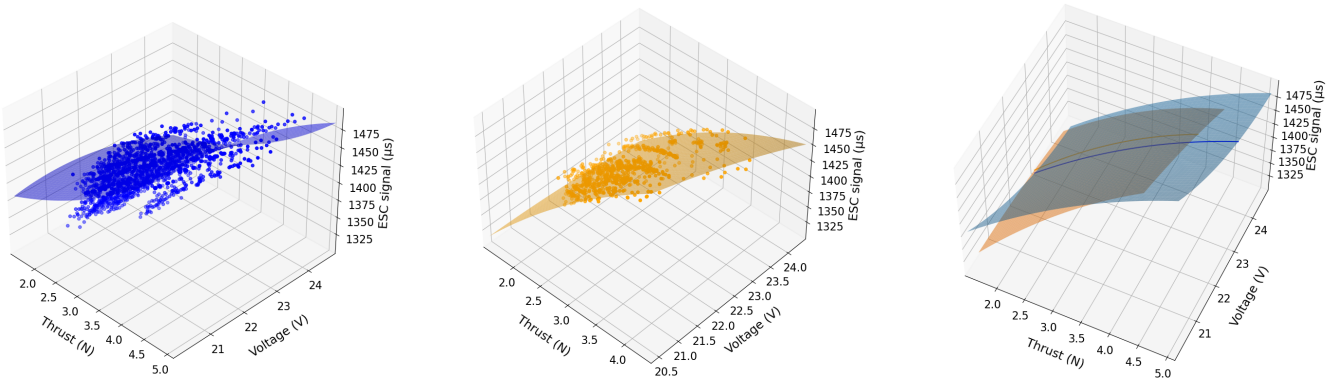

(a) (b) (c)

Figure 6: TM functions fitted from experimental data. 6a shows the polynomial fitted for SR data. 6b shows the polynomial fitted for MR data. 6c shows a comparative between SR (blue) and MR (orange) TMs.

Figure 7 shows the performance of the polynomial fit chosen with the experimental data for the two TMs.

To validate these curves and ensure that the controller did not assume errors derived from the TM, the difference between the measured thrust and the commanded is calculated 14. The results gathered in Table 4 expose that $\gamma(B)$ absorbs the error e_{Th} from the TM and minimizes the error e_T.

$$\hat{e}_T = |T_c - T_m| = |T_c - f(a_z, m)| \tag{14}$$

Finally, the same flights were carried out with fitted correction factor curves added. The results are gathered in Table 4 and show in Figure 8, proving that the previous assumption that the error e_{Th} would be minimized with both TMs is correct.

TM Strategy	e_{Th} (%)	e_T (%)
LA	12.174 ± 1.417	0.538 ± 0.051
SR	4.370 ± 0.744	0.258 ± 0.031
MR	4.934 ± 0.675	0.235 ± 0.030
SR + $\gamma(B)$	0.557 ± 0.313	0.037 ± 0.015
MR + $\gamma(B)$	**0.197 ± 0.357**	**0.007 ± 0.006**

Table 4: e_{Th} and e_T computed for the different strategies. LA: linear approximation. SR: thrust stand with single rotor. MR: thrust stand with multi rotor. SR + $\gamma(B)$: thrust stand with single rotor and correction factor. MR + $\gamma(B)$: thrust stand with multi rotor and correction factor.

5 DISCUSSION

5.1 *Results from thrust stand experiments*

The thrust stand experiments results prove that there is a substantial difference between running the experiments exclusively on one rotor or connecting the other three to the ESC simultaneously. The ESC distributes the power from the battery to the rotors based on the throttle input it receives for each of the rotors. When only one rotor is connected, all the ESC power is dedicated to it. From experimental data, we know that the ESC inputs more than 20A of current to the rotor when it sends a full throttle command. The ESC used in these experiments works up to 65A, which is insufficient to send the needed power of a full throttle command to the four rotors at the same time. Besides, when the four rotors are connected, the same throttle command provokes a larger decay in the battery level, thus obtaining a lower thrust. These differences are shown in Figure 6. The surface corresponding to the MR TM in Figure 6c is at all times above the surface for the SR one. This means that for a given battery level, the MR TM estimates that a higher throttle command is needed to achieve a desired force. Whether this higher computed throttle is more accurate or not is proved in flight experiments.

5.2 *Results from Flight Experiments*

Flight experiments allow to analyze flight performance from the SR and MR TM computed using thrust stand experiments. Throttle and thrust errors from Figures 8 and 9 show that the MR TM has a poorer performance for higher battery levels, above 22.5V, than the SR TM, with a 5% throttle error against the 4% throttle error achieved by SR. Despite this, it has a lower error from 21.5V to the end of the battery duration, as MR throttle error goes down to 4% and SR error goes up to 6%. Looking at the evolution of the battery level in Figure 11, the battery level stays below 23.0V after time reaches 50 seconds, so for the biggest part of flight, the MR TM has a better performance than the SR TM. Even though the mean throttle error of 4.934% for MR TM shown in Table 4 is higher than the one for SR, which is 4.370%, flight experiments show that the MR TM performs a better hover. In Figure 10 it is shown that once the battery level reaches the range of better MR performance, the drone begins to approach the 3 meter reference to hover and improves its flight. However, the SR TM starts to diverge more and more from this reference as the battery runs lower.

http://www.imavs.org/

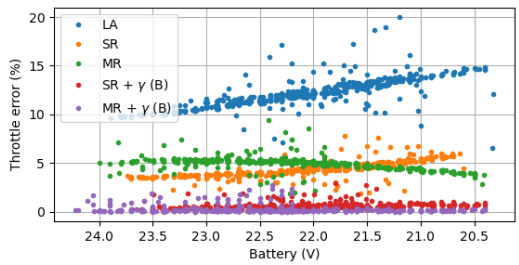

Figure 8: e_{Th} computed for the different TM strategies along the battery range.

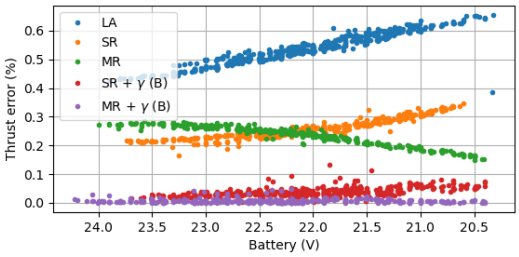

Figure 9: e_T computed for the different TM strategies along the battery range.

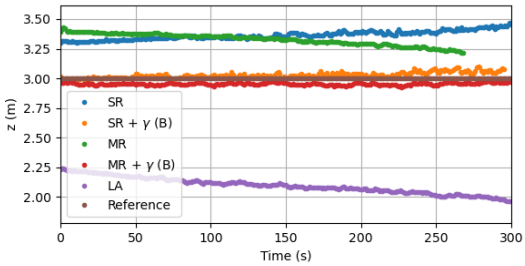

Figure 10: Drone stability performance when commanded to hover at 3 meters height reference for each TM.

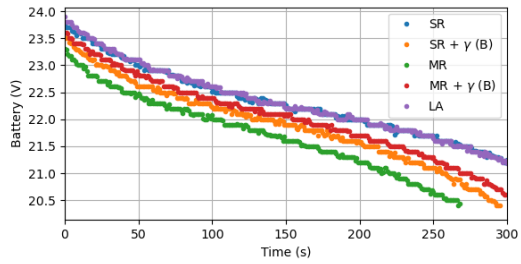

Figure 11: Battery level over time for different strategies

The results for the linear approximation highlight the importance of calibrating a proper TM. This simple solution has an error 10-20 times higher than the other approaches (see Figure 8), and even though it is still possible to fly with such a TM, the trajectory tracking error in the z-axis and the ability to keep hover height are quite poor (see Figure 10).

The addition of a correction factor to previously calibrated TMs is a round success. The throttle error is reduced from 12% to almost 0.5%, as can be seen in Table 4, and the hover error stays within 5 centimeters for a hover reference of 3 m (2%), as shown in Figure 10, throughout the battery range. This error reduction is even higher for the MR+γ TM, achieving a throttle error below 0.2% (see Table 4). This is also due to the MR+γ TM spending more time operating in its most favorable battery range, as previously commented. Despite having lower throttle and thrust errors than SR+γ, the hover performance is very similar, with a hover error also below 2%.

5.3 *Comparative of TMs*

SR and MR error and flight performance can be improved considerably by conducting a couple of flight experiments with which to compute a correction factor that reduces that error to less than 1%. The MR TM has not proven to be as useful as the corrected counterparts. Its mean throttle error increases with respect to the SR one when no correction factor is applied. Figure 6b shows that fewer data were taken from the four rotor experiments, due to the faster discharge of the batteries. This could have affected the accuracy of the MR TM computing. More experiments and more data might result in a better calibration of this MR TM. Even though MR TM shows a slightly better overall hover performance than SR in Figure 10, we consider this improvement not worth the effort to calculate an MR TM alone. When the correction factor was added to the MR TM, the error obtained for the MR + γ proves to be lower than the SR + γ, going down to 0.197%. Although this reduction in the error is significant, the SR+γ shows a good flight performance, with a hover error also within 5cm for a 3 meter hover flight and a throttle error below 1%. We consider the SR+γ TM to be the better strategy in a performance/computation cost relation. TM performance can be slightly improved if MR+γ is a possibility, i.e. if mounting resources and a safe space for experiments are available.

6 CONCLUSION

In this work, we proposed a methodology for Thrust Map estimation that proves to be effective, allowing the estimation of different TMs that predict the forces the drone will produce in real flight experiments.

We also presented an extension to the general approach using a correction factor that is computed from flight data. By applying this correction factor, great improvement is achieved for the in real flight experiments.

Based on these same flight experiments, a comparison of TM calibration strategies was performed, and a TM alternative is proposed as the best overall approach: a Single Rotor with Correction Factor (SR+γ) Thrust Map.

As a proposal for future work, additional TMs can be calibrated using different ESCs and batteries to compare how

http://www.imavs.org/

these components affect the TM for the same set of motors. A change in the motors would undeniably call for a new TM, but the dependency on the selected ESCs and batteries is not so evident.

Additionally, considering how similar the process of fitting a TM or a correction factor to data and computing the error is to the training of an AI agent, these polynomial curves and surfaces fitting can be substituted by machine learning techniques.

ACKNOWLEDGEMENTS

We acknowledge the support of the European Union through the Horizon Europe Project No. HZ230070443 SHEREC: Safe, Healthy and Environmental Ship Recycling and the Horizon Europe Project No. 101070254 CORESENSE. This work has also been supported by Grant ref. ID2021-127648OBC32 INSERTION funded by MICIU/AEI/10.13039/501100011033 and by FEDER, EU. In addition, this work has also been supported by the project RATEC ref: PDC2022-133643-C22 funded by the Spanish Ministry of Science and Innovation. The work of the second author is supported by the Pre-Doctoral Program of Research and Technologic Innovation Department of Madrid Government. The work of the fourth author was funded by the Luxembourg National Research Fund (FNR) under the DEUS Project (Ref.C22/IS/17387634/DEUS).

REFERENCES

[1] Muhammad Maaruf, Magdi Sadek Mahmoud, and Alfian Ma'arif. A survey of control methods for quadrotor uav. *International Journal of Robotics and Control Systems*, 2(4):652–665, 2022.

[2] Yu Wang, Kang Liu, Peiyin Chen, Huiliao Yang, and Di Wang. Adaptive fuzzy fixed-time tracking control for maritime quadrotor uav landing onto a moving usv with deck motion prediction. *Nonlinear Dynamics*, 113(13):16857–16876, 2025.

[3] Paulo Jefferson Dias de Oliveira Evald, Vivian Misaki Aoki, César Bastos da Silva, Dayana Santos Cardoso, Pedro Miranda Pinheiro, Silvia Silva da Costa Botelho, and Paulo Lilles Jorge Drews Junior. A review on quadrotor attitude control strategies. *International Journal of Intelligent Robotics and Applications*, 8(1):230–250, 2024.

[4] Burak Yüksel, Cristian Secchi, Heinrich H Bülthoff, and Antonio Franchi. A nonlinear force observer for quadrotors and application to physical interactive tasks. In *2014 IEEE/ASME international conference on advanced intelligent mechatronics*, pages 433–440. IEEE, 2014.

[5] Bowen Zhang, Zaixin Song, Fei Zhao, and Chunhua Liu. Overview of propulsion systems for unmanned aerial vehicles. *Energies*, 15(2):455, 2022.

[6] Riccardo Spica, Paolo Robuffo Giordano, Markus Ryll, Heinrich H Bülthoff, and Antonio Franchi. An open-source hardware/software architecture for quadrotor uavs. *IFAC Proceedings Volumes*, 46(30):198–205, 2013.

[7] Drew Hanover, Antonio Loquercio, Leonard Bauersfeld, Angel Romero, Robert Penicka, Yunlong Song, Giovanni Cioffi, Elia Kaufmann, and Davide Scaramuzza. Autonomous drone racing: A survey. *IEEE Transactions on Robotics*, 2024.

[8] Matthias Faessler, Davide Falanga, and Davide Scaramuzza. Thrust mixing, saturation, and body-rate control for accurate aggressive quadrotor flight. *IEEE Robotics and Automation Letters*, 2(2):476–482, 2016.

[9] Daniel Hentzen, Thomas Stastny, Roland Siegwart, and Roland Brockers. Disturbance estimation and rejection for high-precision multirotor position control. In *2019 IEEE/RSJ International Conference on Intelligent Robots and Systems (IROS)*, pages 2797–2804. IEEE, 2019.

[10] Zaid Siddiqi and Jin Wook Lee. A computational and experimental study on aerodynamics of motor-driven propellers using thrust stand and rotating cup anemometer. *Progress in Computational Fluid Dynamics, an International Journal*, 22(1):23–36, 2022.

[11] Marián Kišev, Lukáš Vacho, Ladislav Tóth, Martin Olejár, Marta Harničárová, Jan Valíček, Hakan Tozan, et al. Experimental measurement of a uav propeller's thrust. *Tehnički vjesnik*, 29(1):73–80, 2022.

[12] Bart Theys, Grigorios Dimitriadis, Patrick Hendrick, and Joris De Schutter. Influence of propeller configuration on propulsion system efficiency of multi-rotor unmanned aerial vehicles. In *2016 international conference on unmanned aircraft systems (ICUAS)*, pages 195–201. IEEE, 2016.

[13] Rajan Gill and Raffaello D'andrea. Propeller thrust and drag in forward flight. In *2017 IEEE Conference on control technology and applications (CCTA)*, pages 73–79. IEEE, 2017.

[14] Zbigniew Czyż, Paweł Karpiński, Krzysztof Skiba, and Mirosław Wendeker. Wind tunnel performance tests of the propellers with different pitch for the electric propulsion system. *Sensors*, 22(1):2, 2021.

[15] Alexander H Bryant and Dibbon K Walters. Developing a small-scale propeller thrust model using experimentation and cfd. In *AIAA Scitech 2021 Forum*, page 1307, 2021.

[16] C Paz, E Suárez, C Gil, and J Vence. Assessment of the methodology for the cfd simulation of the flight of a quadcopter uav. *Journal of Wind Engineering and Industrial Aerodynamics*, 218:104776, 2021.

[17] Davi Santos, Martin Saska, and Tiago Nascimento. A generalized thrust estimation and control approach for multirotors micro aerial vehicles. *IEEE Robotics and Automation Letters*, 2024.

[18] Du Ho, Jonas Linder, Gustaf Hendeby, and Martin Enqvist. Mass estimation of a quadcopter using imu data. In *2017 International Conference on Unmanned Aircraft Systems (ICUAS)*, pages 1260–1266. IEEE, 2017.

[19] Christoph Böhm, Martin Scheiber, and Stephan Weiss. Filter-based online system-parameter estimation for multicopter uavs. In *Robotics: Science and Systems*, 2021.

[20] Leonard Bauersfeld and Davide Scaramuzza. Range, endurance, and optimal speed estimates for multicopters. *IEEE Robotics and Automation Letters*, 7(2):2953–2960, 2022.

[21] Miguel Fernandez-Cortizas, Martin Molina, Pedro Arias-Perez, Rafael Perez-Segui, David Perez-Saura, and Pascual Campoy. Aerostack2: A software framework for developing multi-robot aerial systems. *arXiv preprint arXiv:2303.18237*, 2023.

http://www.imavs.org/